

DEPARTMENT OF MATHEMATICAL SCIENCES  
COLLEGE OF SCIENCES  
OLD DOMINION UNIVERSITY  
NORFOLK, VIRGINIA 23529

11/16/91  
11/16/91  
11/16/91  
033

**THEORETICAL STUDIES OF LASERS AND CONVERTERS**

By

John H. Heinbockel, Principal Investigator

Progress Report

For the period July 1, 1991 to December 31, 1991

Prepared for

National Aeronautics and Space Administration

Langley Research Center

Hampton, Virginia 23665

Under

**Research Grant NAG-1-757**

Dr. Robert C. Costen, Technical Monitor

SSD-High Energy Science Branch

(NASA-CR-189482) THEORETICAL STUDIES OF  
LASERS AND CONVERTERS Progress Report, 1  
Jul. - 31 Dec. 1991 (Old Dominion Univ.)  
33 p

N92-14333

CSCL 20E

Unclass

G3/36 0053159

November 1991

DEPARTMENT OF MATHEMATICAL SCIENCES  
COLLEGE OF SCIENCES  
OLD DOMINION UNIVERSITY  
NORFOLK, VIRGINIA 23529

**THEORETICAL STUDIES OF LASERS AND CONVERTERS**

By

John H. Heinbockel, Principal Investigator

Progress Report

For the period July 1, 1991 to December 31, 1991

Prepared for

National Aeronautics and Space Administration

Langley Research Center

Hampton, Virginia 23665

Under

**Research Grant NAG-1-757**

Dr. Robert C. Costen, Technical Monitor

SSD-High Energy Science Branch

!

November 1991

**PROGRESS REPORT NASA GRANT NAG1-757  
ODURF 176615**

**THEORETICAL STUDIES OF LASERS AND CONVERTERS**

We have previously examined Doppler broadening and its effects upon the stimulated emission cross-section  $\sigma_{ij}$  connecting an upper level ( $i$ ) with a lower level ( $j$ ) for an iodine laser. The stimulated emission cross-section is given by (reference 1),

$$\sigma_{ij} = \frac{\lambda^2 A_{ij}}{8\pi} g_{ij}(\nu) \quad (1)$$

where,  $g_{ij}(\nu)$  is the normalized line shape function

$$g_{ij}(\nu) = \frac{2}{\pi \Delta\nu \left( 1 + 4 \left[ \frac{\nu - \nu_{ij}}{\Delta\nu} \right]^2 \right)}. \quad (2)$$

The level transitions for the iodine laser are illustrated in the figure 1. The relative intensities of these transitions are illustrated in figure 2.

The Einstein coefficients for the different lines have the transition rates

$$\begin{array}{ll} A_{34} = 5.0\alpha & A_{23} = 2.3\alpha \\ A_{33} = 2.1\alpha & A_{22} = 3.0\alpha \\ A_{32} = 0.6\alpha & A_{21} = 2.4\alpha \end{array} \quad (3)$$

in units of  $\text{sec}^{-1}$ , where  $\alpha = A/7.77$  with  $A = 5.4 \pm 2.0 \text{sec}^{-1}$ . Using

$$\nu_0 = \frac{c}{1.315246(10)^{-4}} = 2.28094(10)^{14} \approx 2.3(10)^4 \text{ GHz}, \quad (4)$$

the laser emission frequencies from  $\nu_0$  are given by

$$\begin{array}{ll} \nu_{34} = \nu_0 & \nu_{21} = \nu_0 - 0.427c \\ \nu_{33} = \nu_0 + 0.141c & \nu_{22} = \nu_{21} - 0.026c \\ \nu_{32} = \nu_{33} + 0.068c & \nu_{23} = \nu_{22} - 0.068c \end{array} \quad (5)$$

and consequently the overall stimulated emission cross-section is given by

$$\sigma = \frac{\lambda^2}{4\pi^2 \Delta\nu} \left\{ \frac{5}{12} \sum_{i=1}^3 \frac{A_{2i}}{1 + \left[ 2 \left( \frac{\nu - \nu_{2i}}{\Delta\nu} \right) \right]^2} + \frac{7}{12} \sum_{i=2}^4 \frac{A_{3i}}{1 + \left[ 2 \left( \frac{\nu - \nu_{3i}}{\Delta\nu} \right) \right]^2} \right\} \quad (6)$$

which is based upon statistical weights of the hyperfine levels (reference 1) and

$$\Delta\nu = \alpha_0 + \alpha_1 p \quad (7)$$

with  $\alpha_0 = 2.51(10)^8 \sqrt{T/300}$ ,  $\alpha_1 = 1.88(10)^7 \sqrt{T/300}$ , where  $p$  is the pressure in torr, and  $T$  is the temperature in degrees Kelvin. Here  $\alpha_0$  is related to the Doppler line width and  $\alpha_1$  is the pressure broadening coefficient associated with the laser  $n - C_3F_7I$ .

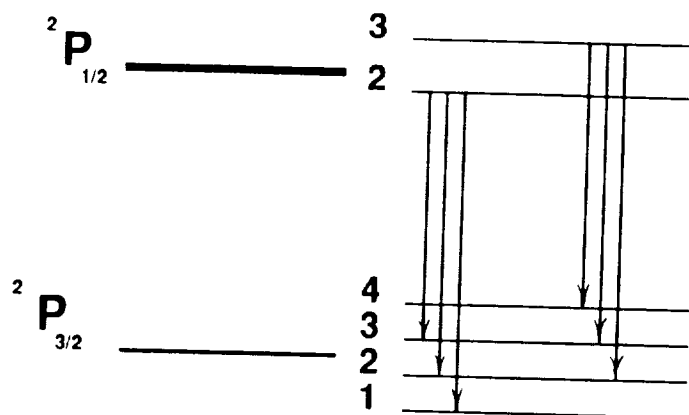


Figure 1. Level transitions for iodine.

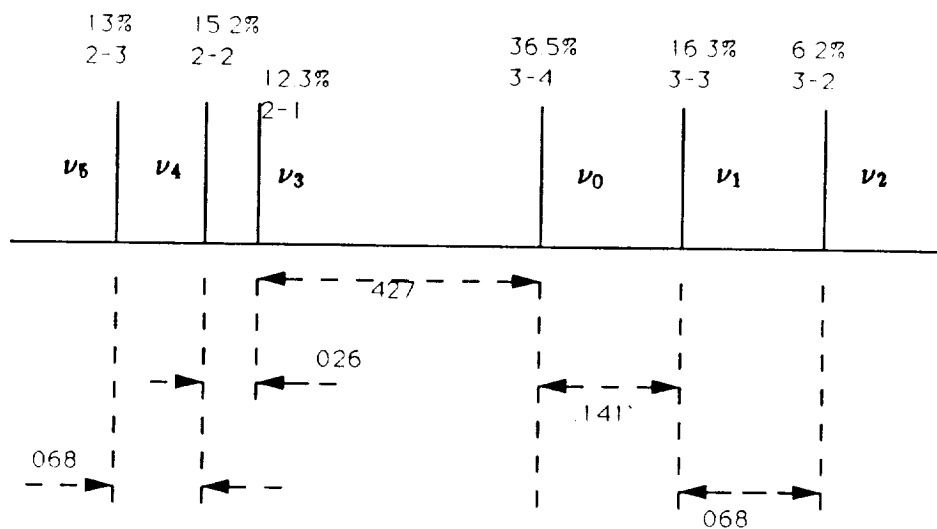


Figure 2. Relative intensities for iodine transitions

## The Voigt Profile

The Voigt profile considers the effect of both Doppler broadening and collision broadening upon the absorption line shape. For homogeneous broadening it is assumed that every atom behaves in the same way. In this case the line shape function has a Lorentzian form. If a select group of atoms emit a frequency  $\nu_{ij}$  in their rest frame and the rest frame moves with velocity  $v_z$ , then their emits a Doppler shift frequency and line shape function for the group. In particular, a group of atoms identified with a velocity component  $v_z$  has the shifted line shape function (references 2,3)

$$g(\nu, v_z) = \frac{2}{\pi \Delta\nu \left( 1 + 4 \left[ \frac{\nu - \nu_{ij} + \nu_{ij} \frac{v_z}{c}}{\Delta\nu} \right]^2 \right)} \quad (8)$$

where the fraction of atoms within the velocity range  $v_z$  and  $v_z + dv_z$  is given by the Maxwell-Boltzmann distribution

$$\frac{dN}{N} = \left( \frac{M}{2\pi kT} \right)^{1/2} \exp \left( \frac{-Mv_z^2}{2kT} \right) dv_z \quad (9)$$

Multiplying equations (8) and (9) and integrating over all velocities, produces the Voigt profile line shape function

$$g_{ij}(\nu) = \left( \frac{M}{2\pi kT} \right)^{1/2} \int_{-\infty}^{\infty} \left\{ \frac{2}{\pi \Delta\nu \left( 1 + 4 \left[ \frac{\nu - \nu_{ij} + \nu_{ij} \frac{v_z}{c}}{\Delta\nu} \right]^2 \right)} \right\} \exp \left( \frac{-Mv_z^2}{2kT} \right) dv_z$$

or

$$g_{ij}(\nu) = \left( \frac{M}{2\pi kT} \right)^{1/2} \int_{-\infty}^{\infty} \frac{2\Delta\nu \exp \left( \frac{-Mv_z^2}{2kT} \right) dv_z}{\pi [(\Delta\nu)^2 + 4(\nu - \nu_{ij} + \nu_{ij} \frac{v_z}{c})^2]} \quad (10)$$

The above integral is simplified by making the change of variables

$$y^2 = \frac{Mv_z^2}{2kT} \quad dy = \left( \frac{M}{2kT} \right)^{1/2} dv_z \quad (11)$$

$$c_{ij} = 2\nu_{ij} \left( \frac{2kT \ln 2}{Mc^2} \right)^{1/2} \quad (12)$$

$$b_{ij} = (\ln 2)^{1/2} \frac{\Delta\nu}{c_{ij}} \quad (13)$$

$$x_{ij} = 2(\ln 2)^{1/2} \frac{\nu - \nu_{ij}}{c_{ij}} \quad (14)$$

We can then express the line shape function in the form

$$g_{ij}(\nu) = \frac{2}{\pi^{1/2} \Delta\nu} \int_{-\infty}^{\infty} \frac{\ln 2 \left( \frac{\Delta\nu}{c_{ij}} \right)^2 e^{-y^2} dy}{\pi \left[ \ln 2 \left( \frac{\Delta\nu}{c_{ij}} \right)^2 + \left( \frac{2(\nu - \nu_{ij})(\ln 2)^{1/2}}{c_{ij}} + \frac{2\nu_{ij} v_z (\ln 2)^{1/2}}{c c_{ij}} \right)^2 \right]}. \quad (15)$$

Observe that

$$\frac{2\nu_{ij} v_z (\ln 2)^{1/2}}{c c_{ij}} = v_z \left( \frac{M}{2kT} \right)^{1/2} = y \quad (16)$$

and consequently we obtain the simplification

$$g_{ij}(\nu) = \frac{2}{\pi^{3/2} \Delta\nu} \int_{-\infty}^{\infty} \frac{e^{-y^2} dy}{1 + \left( \frac{x_{ij} + y}{b_{ij}} \right)^2}. \quad (17)$$

The overall stimulated emission cross-section is then given by

$$\sigma = \frac{\lambda^2}{8\pi} \left\{ \frac{5}{12} (A_{21}g_{21} + A_{22}g_{22} + A_{23}g_{23}) + \frac{7}{12} (A_{32}g_{32} + A_{33}g_{33} + A_{34}g_{34}) \right\} \quad (18)$$

The figures 3,4,5 and 6 are graphs of  $\sigma$  vs frequency change from  $\nu_0$  for pressures of 5, 30, 80 and 160 torr and temperature of 293 K.

The equations describing the Voigt profile have been added to the continuous flow laser model laser simulation program. The results have been compared with the standard absorption profile reported in an earlier study. There seems to be no advantage to using the Voigt profile as the laser power output is relatively insensitive to changes in the absorption cross section at the pressures being considered for a space laser. One disadvantage of using the Voigt profile is the excessive numerical computations required by the additional equations.

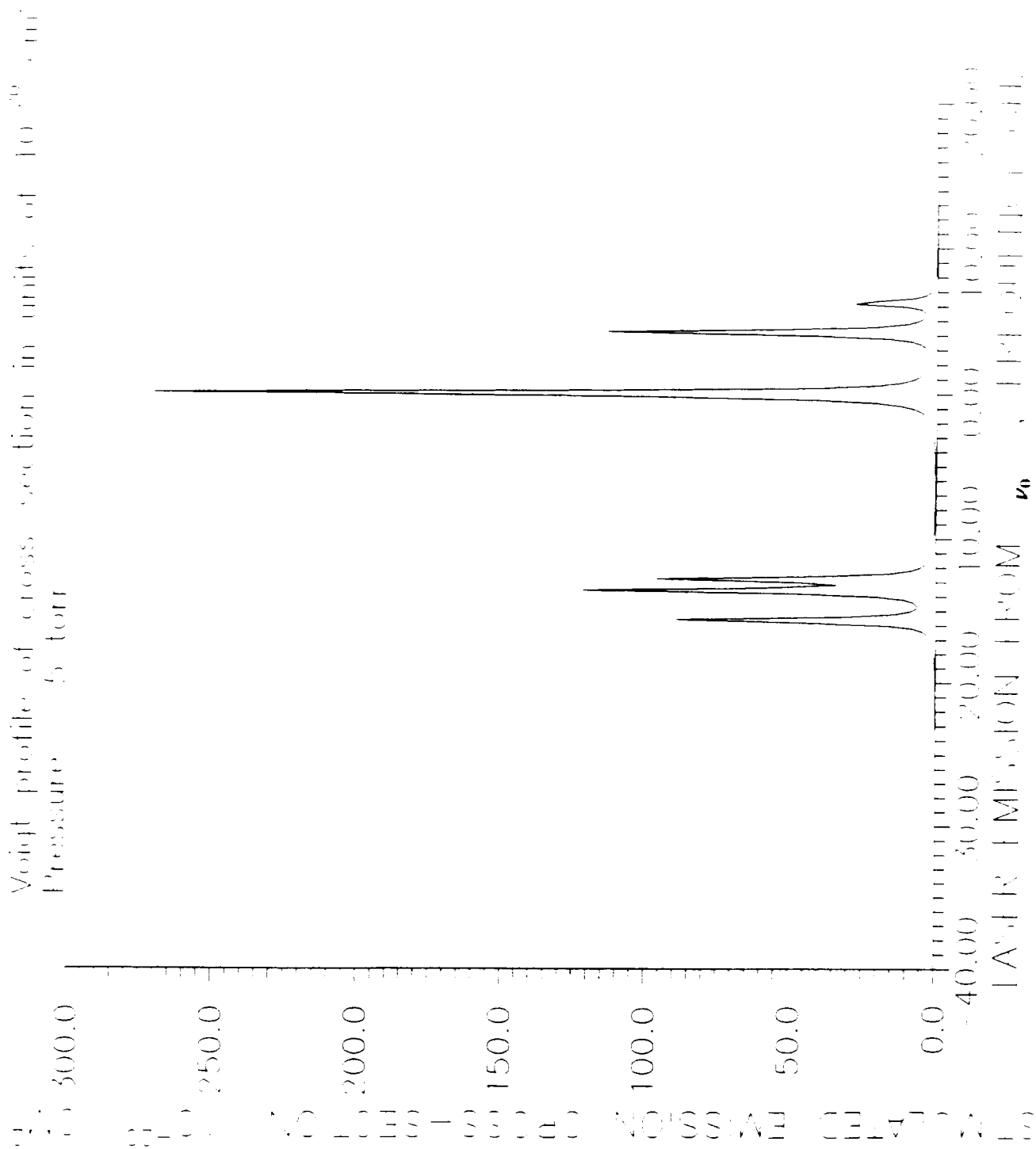


Figure 3 Stimulated emission cross-section  $(10)^{-20} \text{ cm}^2$   
 vs laser emission from  $\nu_0$ , frequency GHz with pressure of 5 torr

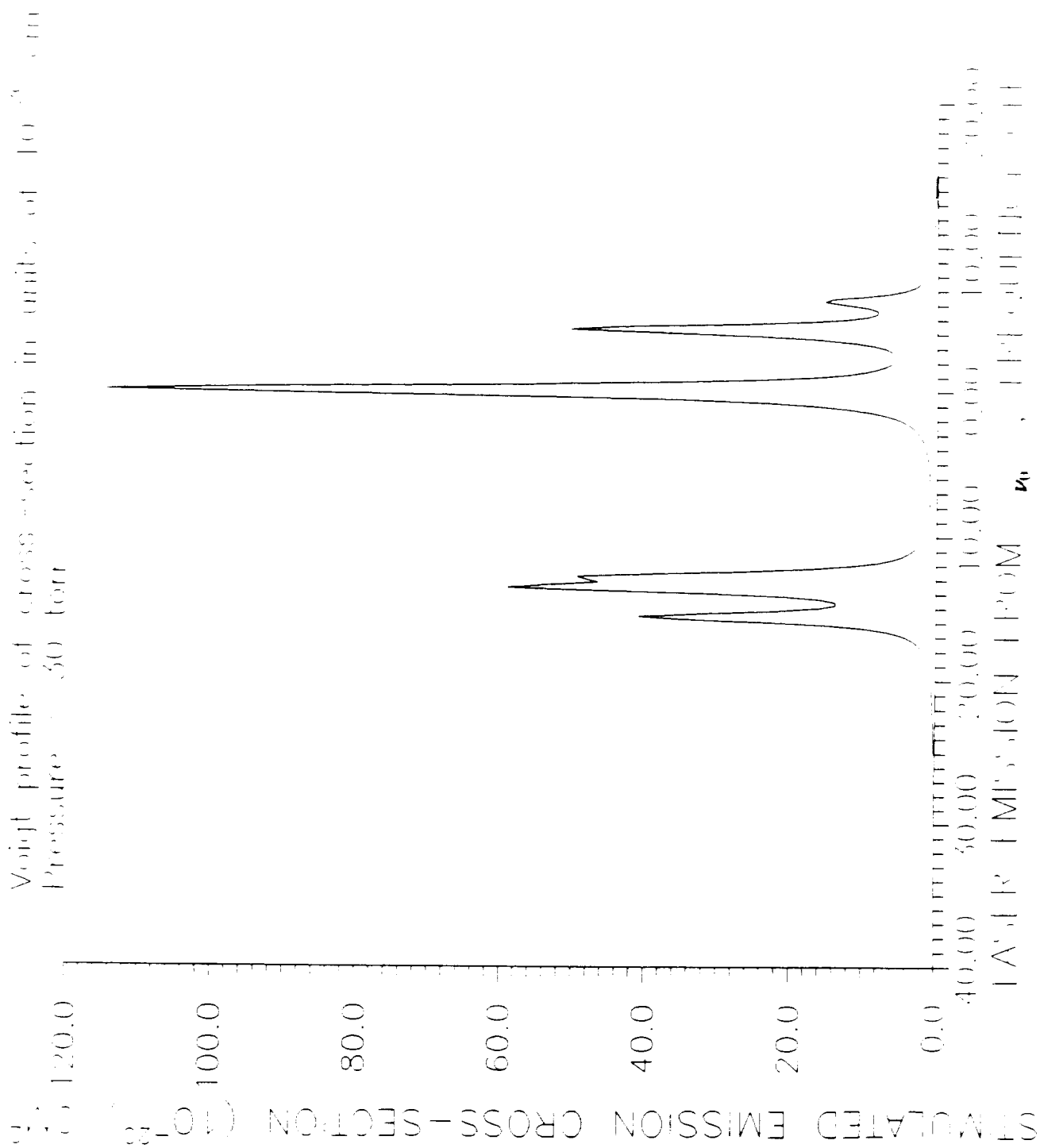


Figure 4 Stimulated emission cross-section  $(10)^{-20} \text{ cm}^2$   
vs laser emission from  $\nu_0$ , frequency GHz with pressure of 30 torr



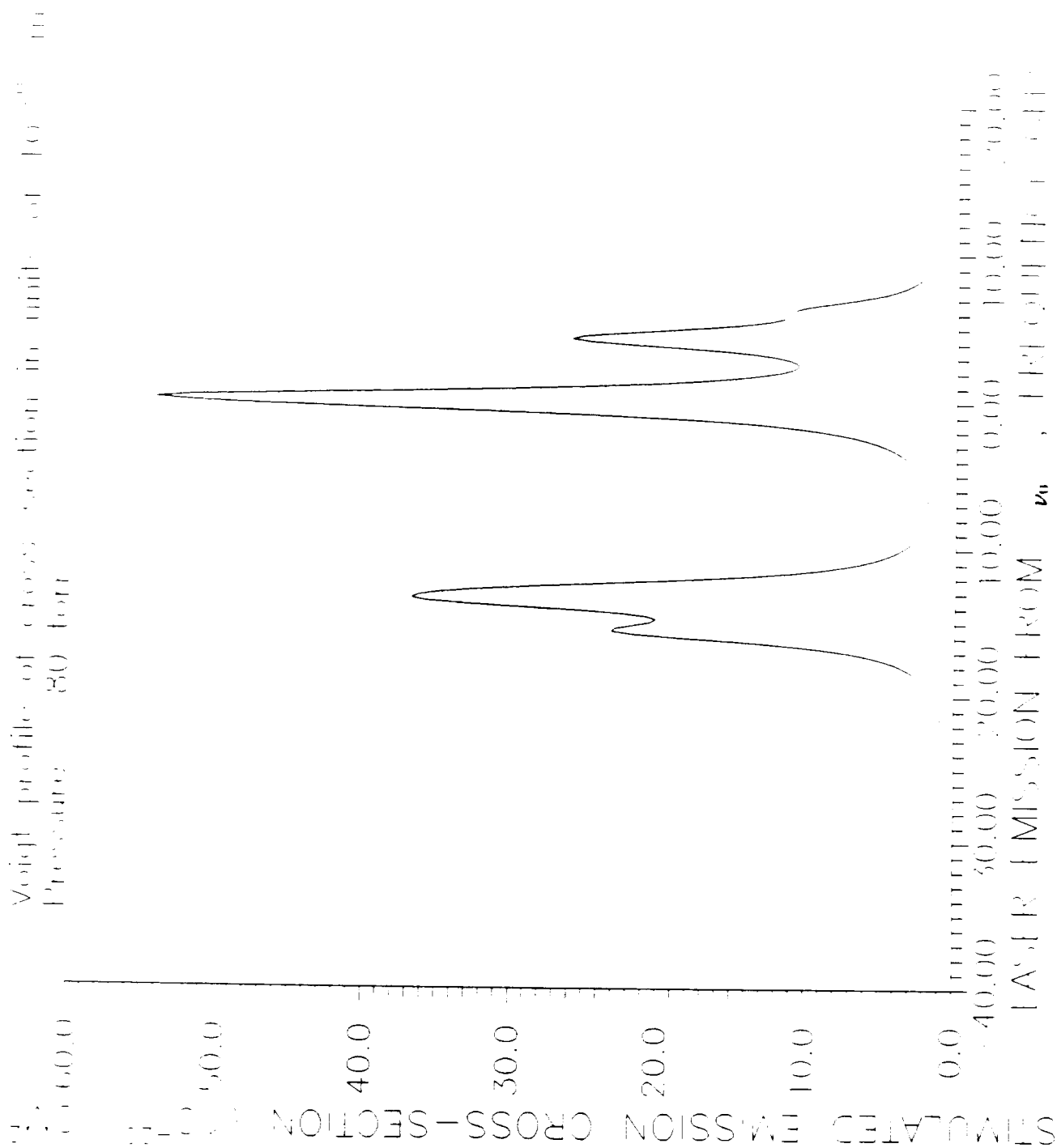


Figure 5 Stimulated emission cross-section  $(10)^{-20} \text{ cm}^2$   
vs laser emission from  $\nu_0$ , frequency GHz with pressure of 80 torr

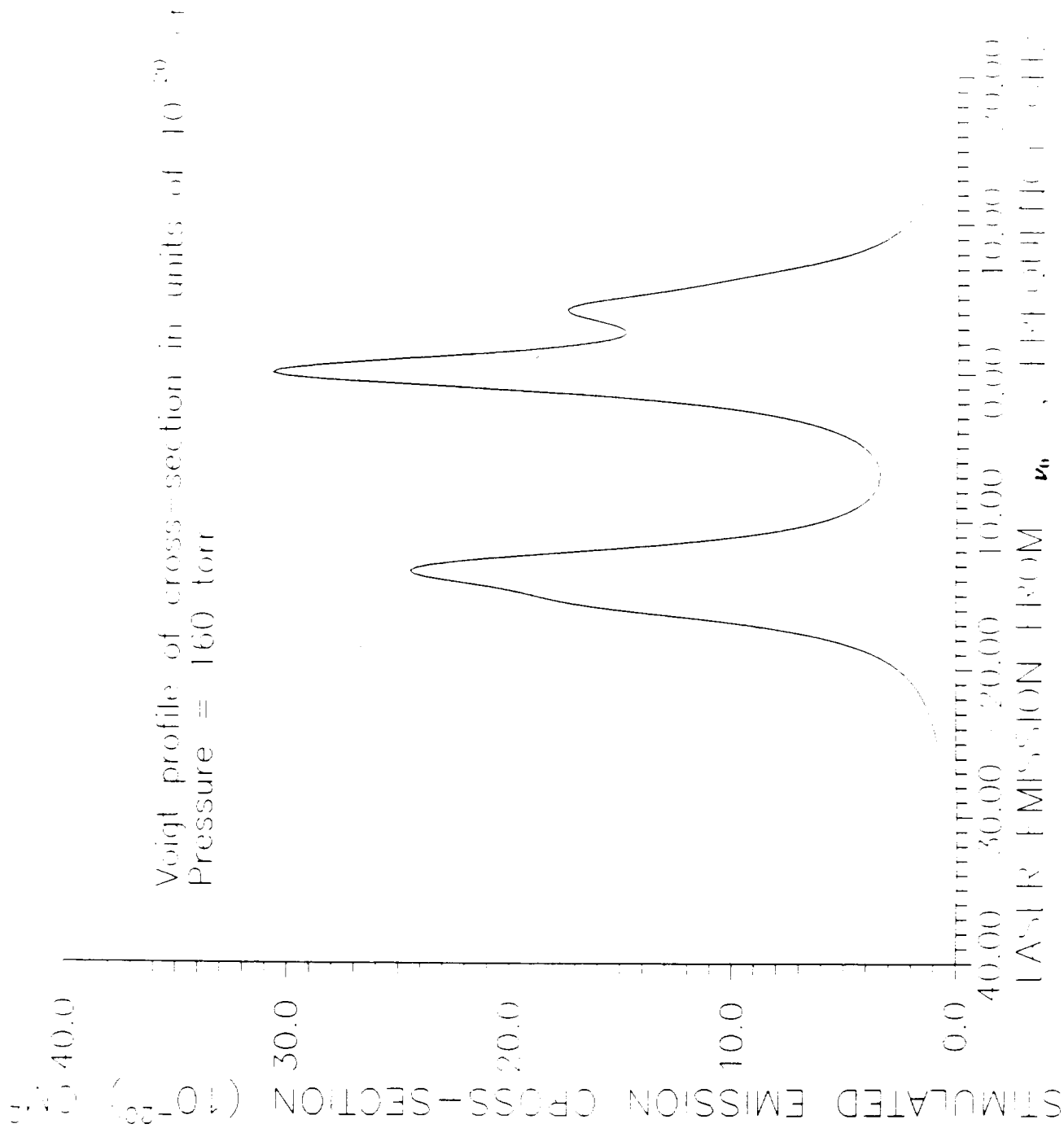


Figure 6 Stimulated emission cross-section  $(10)^{-20} \text{ cm}^2$   
vs laser emission from  $\nu_0$ , frequency GHz with pressure of 160 torr

## SIMULATIONS

The current version of the continuous flow laser model computer program was used to compare results from the model with experimental results. The Appendix A contains a fit with the experimental data obtained for the perfluoride  $i - C_3F_7I$ . The Appendix B contains a fit with the experimental data obtained for the perfluorides  $n - C_3F_7I$  and  $n - C_4F_9I$ .

The Appendix C contains a simulation, using the laser model, for a  $t - C_4F_9$  space laser which is 5 meters in length. The simulation assumes the laser is fully pumped and operating at a pressure of 3.6 torr with a solar concentration of 1370 S.C.

The parameters listed in the Appendices have the following meanings: PTO is the pressure in torr; R2 is reflectivity coefficient of output mirror; OMEG1 is flow velocity upon entering laser; CON is the concentration is solar constants; LC is the length of the laser; ZOL is the half length of the pumped region; T0 is the initial inlet gas temperature; A is the laser radius in cm;  $0 \leq XNRHO \leq 1$  is the fraction of incident pump energy left after geometry considerations; FRAC is the fraction of incident radiation energy converted to heat and thermodynamic effects; RAD is the radius along which the numerical integrations were performed; CHI1 is the photo dissociation rate at a given wavelength; CHI2 is the photo dissociation rate at another wavelength; CHI3 is postulated third photo dissociation rate (assumed zero for all fits with experimental data); A00,B00 are coefficients used to calculate the perfluoride specific heats at constant volume; KK1 through KK10 are reaction rates; QQ1 through QQ5 are quenching coefficients; and CC1 through CC4 are three body collision reaction rates.

## Bibliography

- [1] G. Brederlow, E. Fill, K.J. White, The High-Power Iodine Laser, Springer-Verlag, Berlin, Heidelberg, New York, 1983.
- [2] P.W. Milonni, J.A. Eberly, Lasers, John Wiley, 1988.
- [3] J.T. Verdeyen, Laser Electronics, Prentice-Hall, 1989.

APPENDIX A: EXPERIMENTAL AND THEORETICAL CURVES FOR  $i\text{-C}_3\text{F}_7\text{I}$

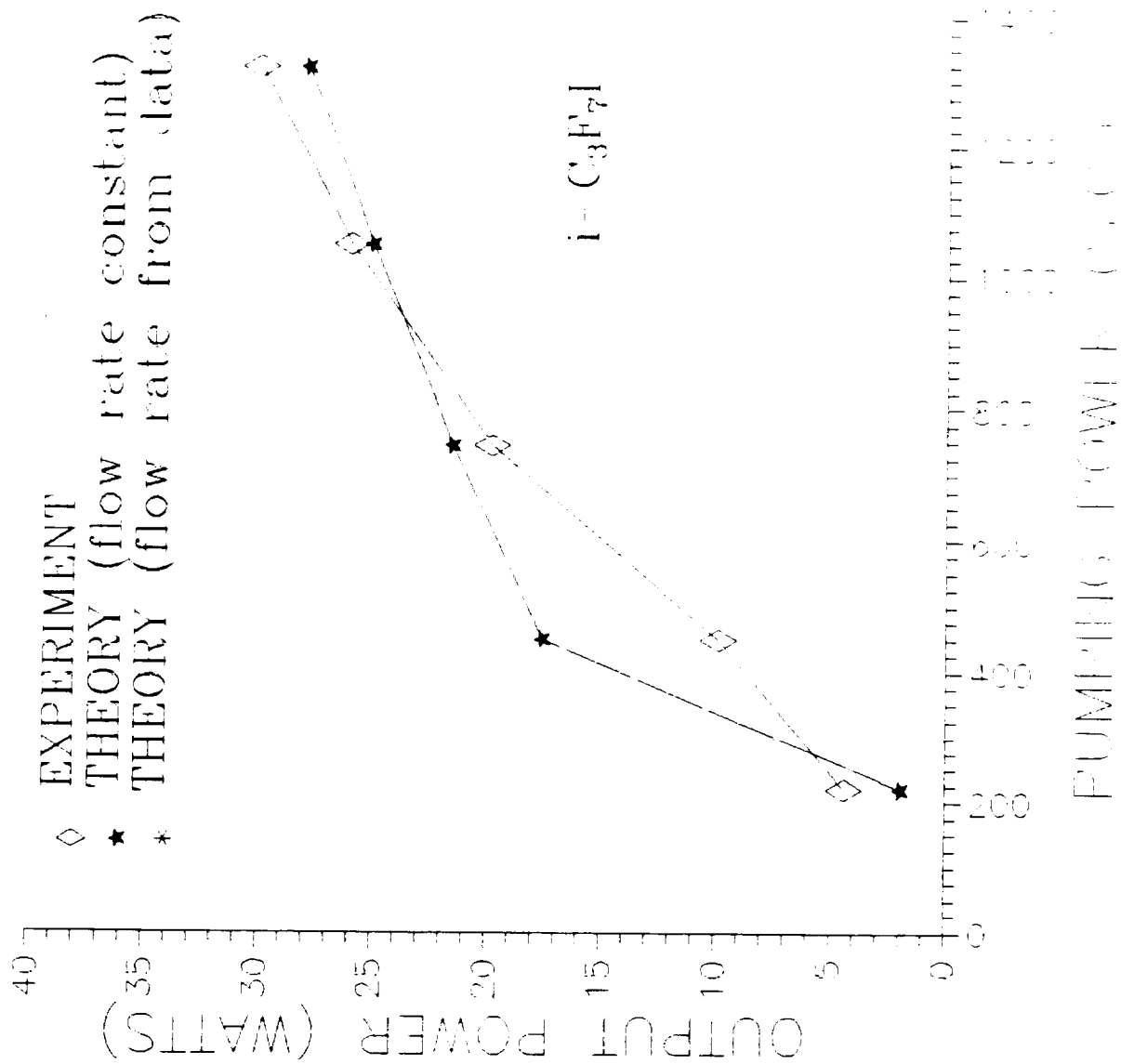


Figure A1 Output power vs pumping power for  $i\text{-C}_3\text{F}_7\text{I}$ .

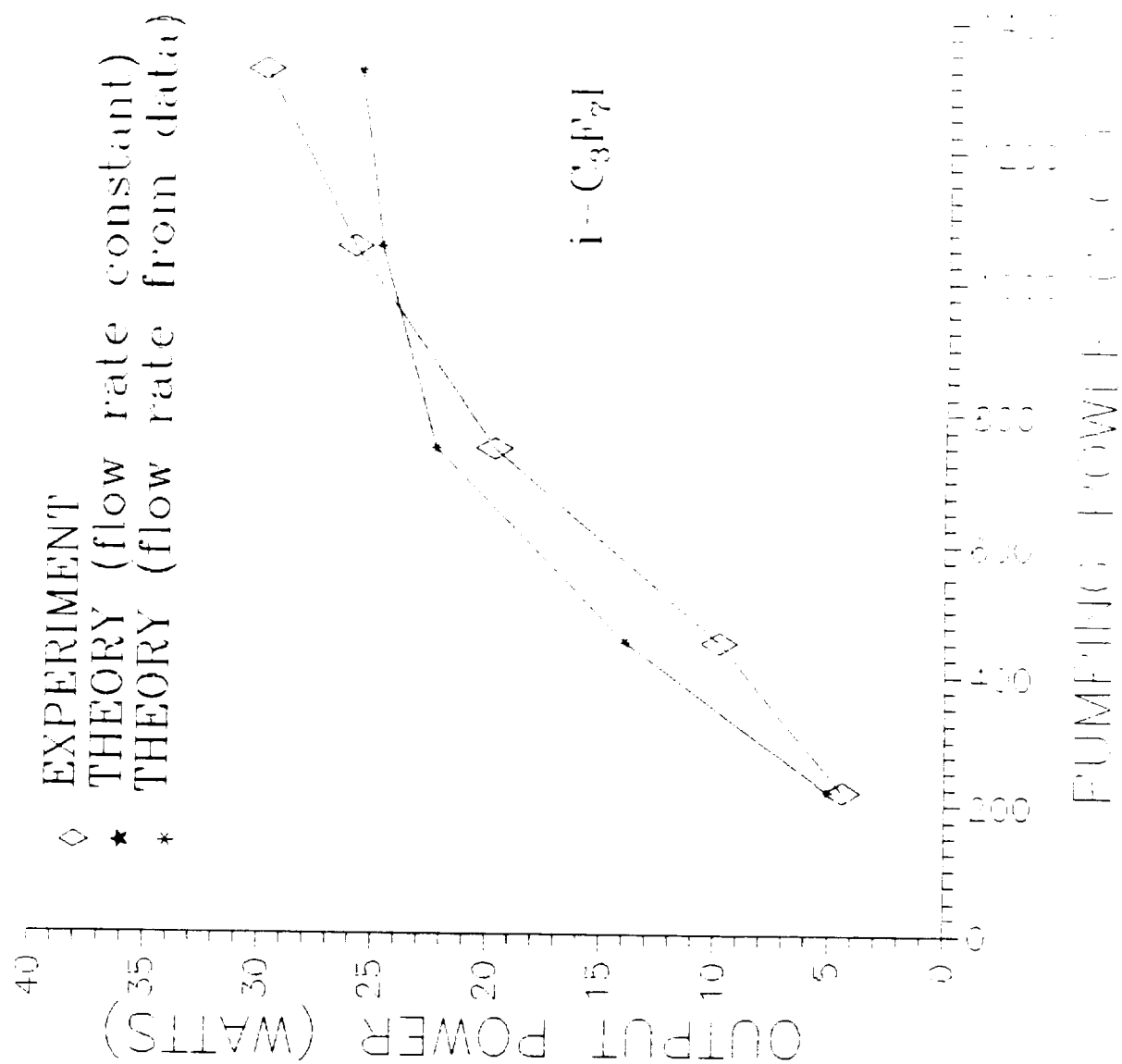


Figure A2 Output power vs pumping power for  $i\text{-C}_3\text{F}_7\text{I}$ .

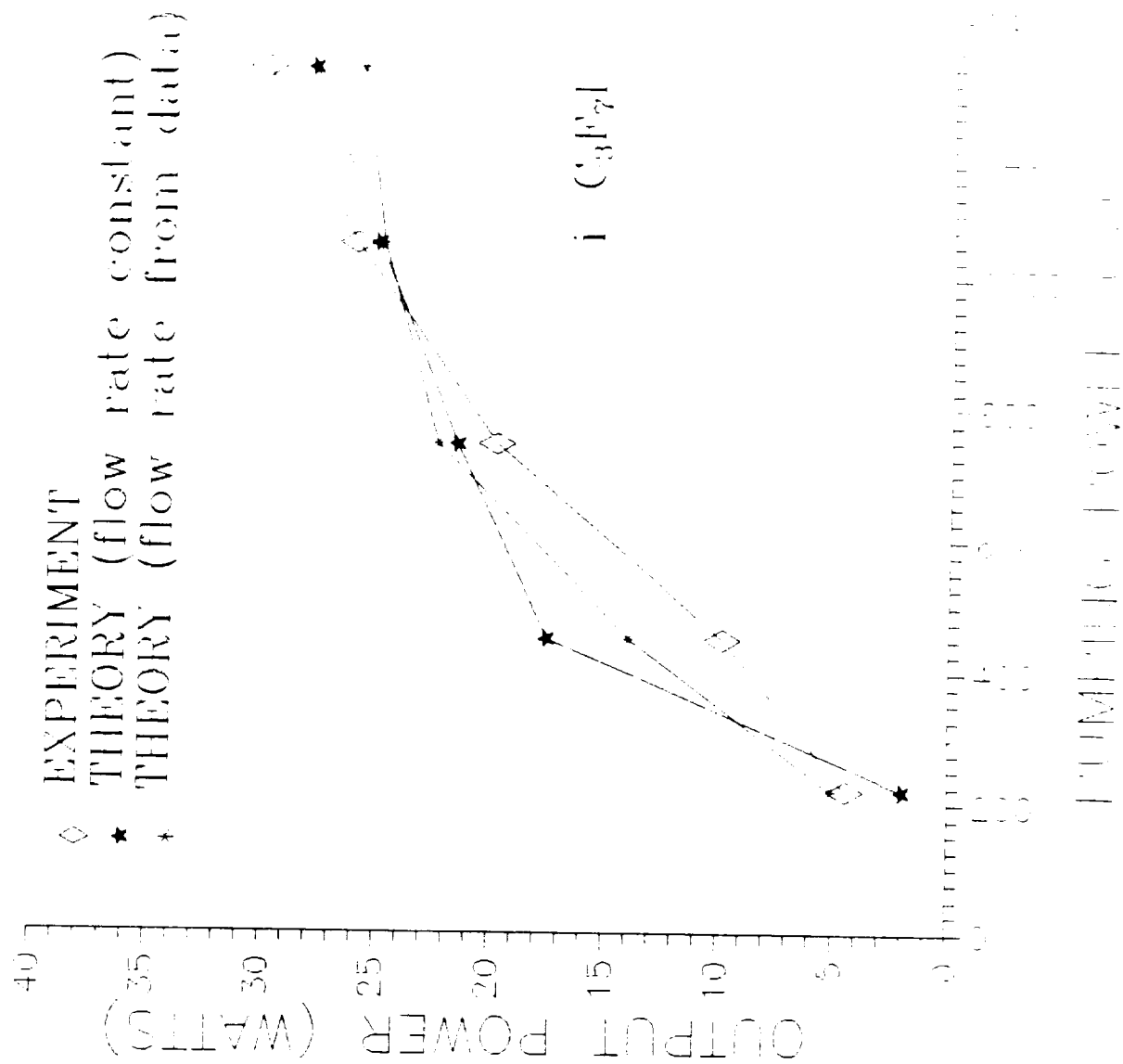


Figure A3 Output power vs pumping power for  $i\text{-C}_3\text{F}_7\text{I}$ .



# PARAMETERS

		Experimental Concentration	Power (Watts)	Calculated Power (Watts)
PT0 =	3.580000			
OMEG1 =	363.200000			
C00 =	3.900000E+18			
R1 =	1.000000	220	4.42	5.05
R2 =	8.500000E-01	450	9.86	14.7
TM =	1.500000E-01	745	19.8	23.65
XNRHO =	1.000000	1050	26	26.02
CON =	220.000000	1320	30	27.2
LC =	15.000000			
ZOL =	7.500000			
A =	1.850000			
R20 =	0.000000E+00			
FRAC =	4.500000E-04			
T0 =	300.000000			
RAD =	0.000000E+00			
V1 =	0.000000E+00			
V2 =	0.000000E+00			
TTT2 =	1.000000E+18			
TTT3 =	1.000000E+18			
TTT4 =	1.000000E+18			
TTT5 =	1.000000E+18			
TTT6 =	1.000000E+18			
CHI1 =	1.200000E-02			
CHI2 =	1.200000E-01			
CHI3 =	0.000000E+00			
KK1 =	1.000000E-14			
KK2 =	2.300000E-11			
KK3 =	6.500000E-13			
KK4 =	3.000000E-16			
KK5 =	5.000000E-11			
KK6 =	0.000000E+00			
KK7 =	3.000000E-19			
KK8 =	1.600000E-23			
KK9 =	1.000000E+15			
KK10 =	1.000000E+17			
AA0 =	147.230000			
BB0 =	1.200000E-03			
CC1 =	1.600000E-33			
CC2 =	5.700000E-33			
CC3 =	0.000000E+00			
CC4 =	1.000000			
CC5 =	8.000000E-33			
QQ1 =	1.700000E-17			
QQ2 =	2.890000E-11			
QQ3 =	3.700000E-18			
QQ4 =	4.700000E-16			
QQ5 =	1.600000E-14			

ORIGINAL PAGE IS  
OF POOR QUALITY

APPENDIX B: EXPERIMENTAL AND THEORETICAL CURVES FOR  $n\text{-C}_3\text{F}_7\text{I}$  and  
 $t\text{-C}_4\text{F}_9\text{I}$

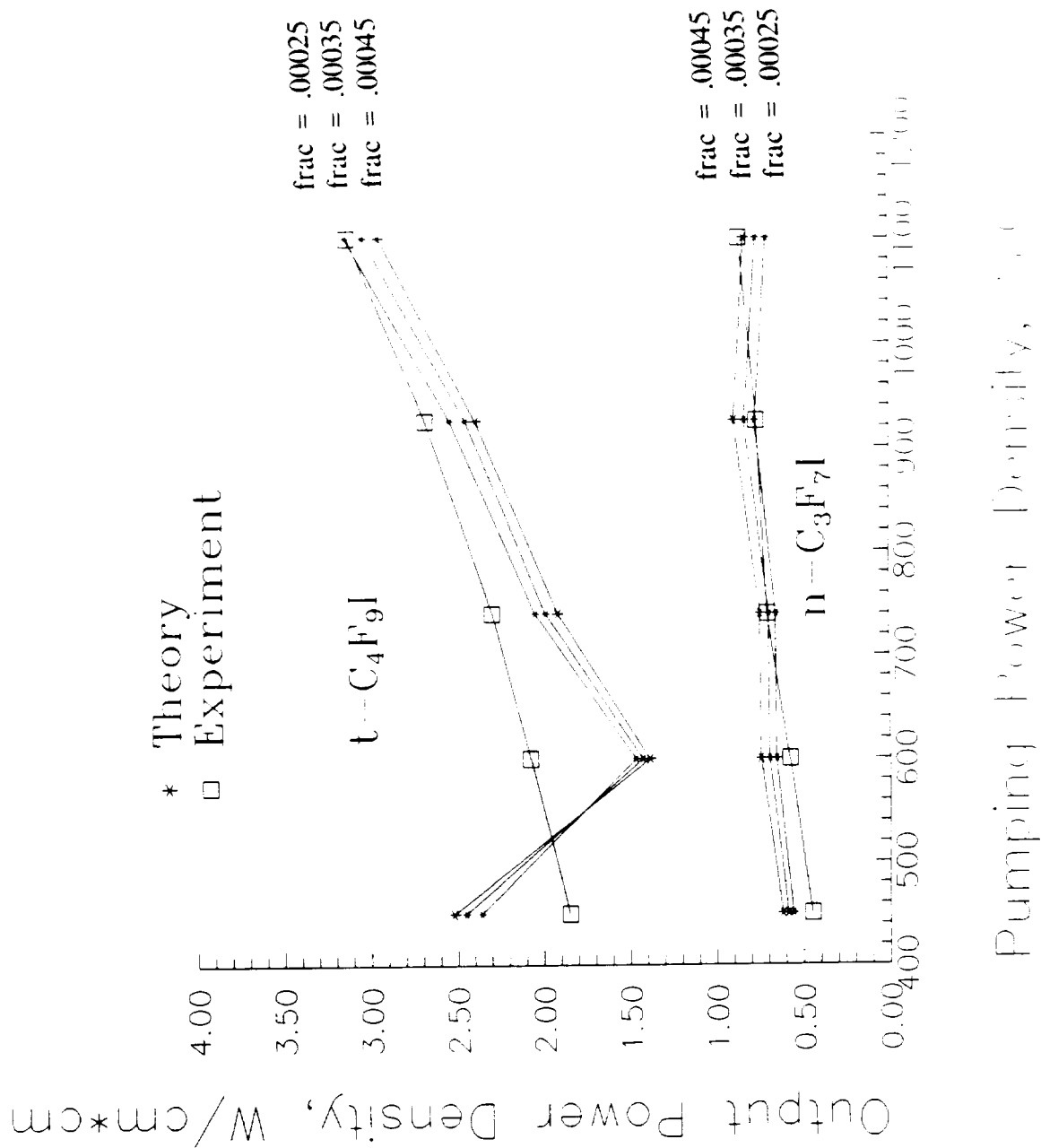


Figure B1 Output power vs pumping power for n-C<sub>3</sub>F<sub>7</sub>I and t-C<sub>4</sub>F<sub>9</sub>I.

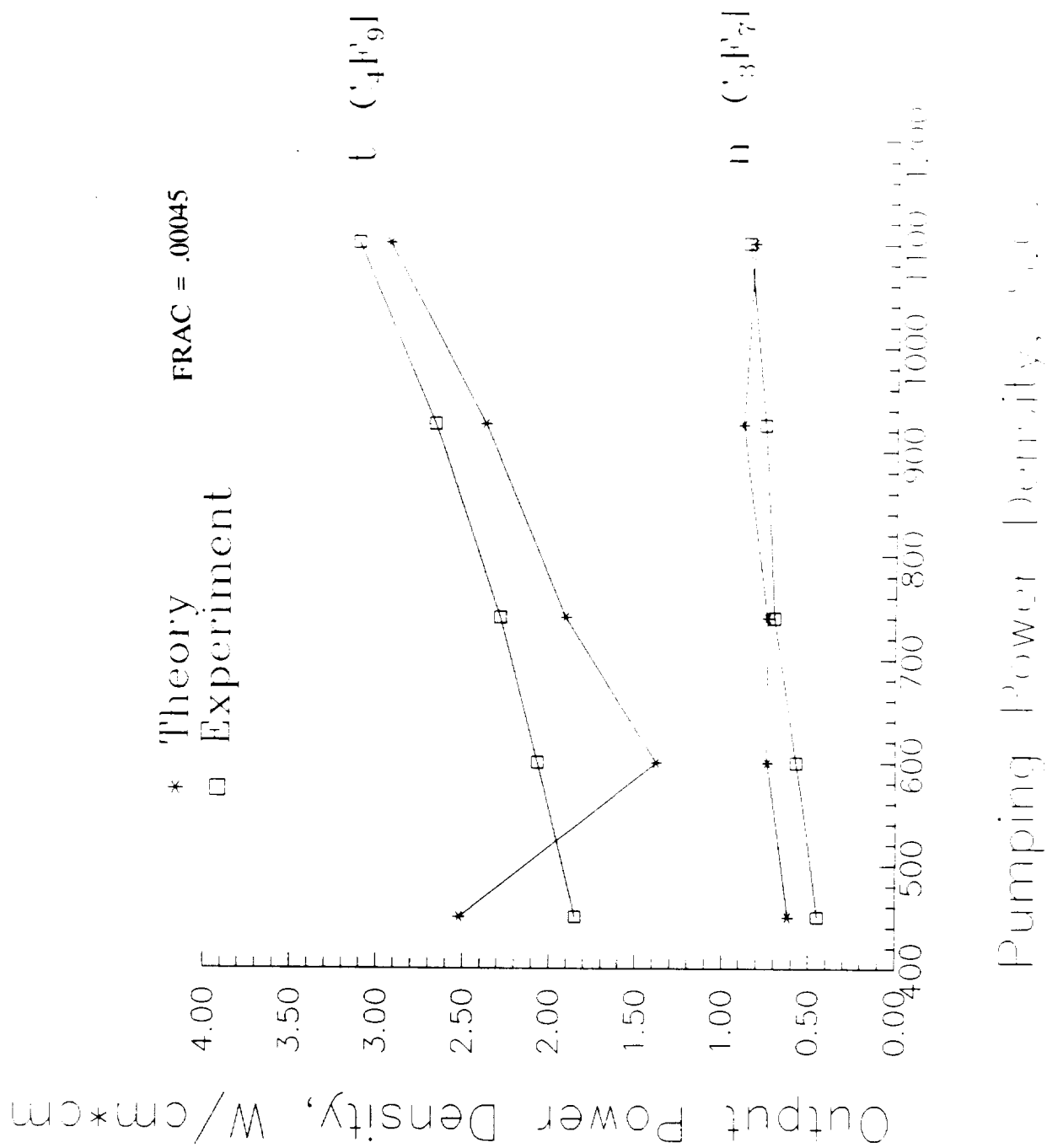


Figure B2 Output power vs pumping power for n-C<sub>3</sub>F<sub>7</sub>I and t-C<sub>4</sub>F<sub>9</sub>I.

## n-C3F7I

```

R1 =      1.000000
R2 =      7.000000E-01
TM =      3.000000E-01
XNRHO =      1.000000
LC =      15.000000
ZOL =      7.500000
A =      1.000000
R20 =      0.000000E+00
FRAC =      4.500000E-04
T0 =      300.000000
RAD =      0.000000E+00
V1 =      0.000000E+00
V2 =      0.000000E+00
TTT2 =      1.000000E+18
TTT3 =      1.000000E+18
TTT4 =      1.000000E+18
TTT5 =      1.000000E+18
TTT6 =      1.000000E+18
CHI1 =      1.200000E-02
CHI2 =      1.200000E-01
CHI3 =      0.000000E+00
KK1 =      1.000000E-14
KK2 =      2.300000E-11
KK3 =      2.000000E-12
KK4 =      3.000000E-16
KK5 =      1.000000E-11
KK6 =      0.000000E+00
KK7 =      3.000000E-19
KK8 =      1.600000E-23
KK9 =      1.000000E+15
KK10 =      1.000000E+17
AA0 =      147.230000
BB0 =      1.200000E-03
CC1 =      1.600000E-33
CC2 =      5.700000E-33
CC3 =      0.000000E+00
CC4 =      1.000000
CC5 =      8.000000E-33
QQ1 =      1.700000E-17
QQ2 =      2.890000E-11
QQ3 =      3.700000E-18
QQ4 =      4.700000E-16
QQ5 =      1.600000E-14

```

## t-C4F9I

```

R1 =      1.000000
R2 =      7.000000E-01
TM =      3.000000E-01
XNRHO =      1.000000
LC =      15.000000
ZOL =      7.500000
A =      1.000000
R20 =      0.000000E+00
FRAC =      4.500000E-04
T0 =      300.000000
RAD =      0.000000E+00
V1 =      0.000000E+00
V2 =      0.000000E+00
TTT2 =      1.000000E+18
TTT3 =      1.000000E+18
TTT4 =      1.000000E+18
TTT5 =      1.000000E+18
TTT6 =      1.000000E+18
CHI1 =      1.320000E-02
CHI2 =      1.200000E-01
CHI3 =      0.000000E+00
KK1 =      1.000000E-14
KK2 =      6.000000E-12
KK3 =      3.000000E-14
KK4 =      3.000000E-18
KK5 =      1.000000E-11
KK6 =      0.000000E+00
KK7 =      3.000000E-19
KK8 =      1.600000E-23
KK9 =      1.000000E+14
KK10 =      1.000000E+16
AA0 =      183.262400
BB0 =      1.398680E-03
CC1 =      1.600000E-33
CC2 =      5.700000E-33
CC3 =      0.000000E+00
CC4 =      1.000000
CC5 =      8.000000E-33
QQ1 =      6.100000E-17
QQ2 =      2.890000E-11
QQ3 =      3.700000E-18
QQ4 =      4.700000E-16
QQ5 =      1.600000E-14

```

P	n-C3F7I CON	OMEG1	POWER DENSITY
	5.6      450	663	0.62
	5.6      600	663	0.74
	6        740	619	0.74
	5.8      925	640	0.89
	6.4     1100	580	0.83

P	t-C4F9I CON	OMEG1	POWER DENSITY
	9        450	550	2.52
	4.5      600	733	1.38
	4.5      740	733	1.91
	4.2      925	707	2.38
	4.2     1100	707	2.94

APPENDIX C: SIMULATION OF  $t\text{-C}_4\text{F}_9\text{I}$  FIVE METER SPACE LASER, FULLY  
PUMPED OPERATING AT 3.6 TORR WITH A SOLAR  
CONCENTRATION OF 1370 SOLAR CONSTANTS

# Simulated t-C<sub>4</sub>F<sub>9</sub>I Space Layer

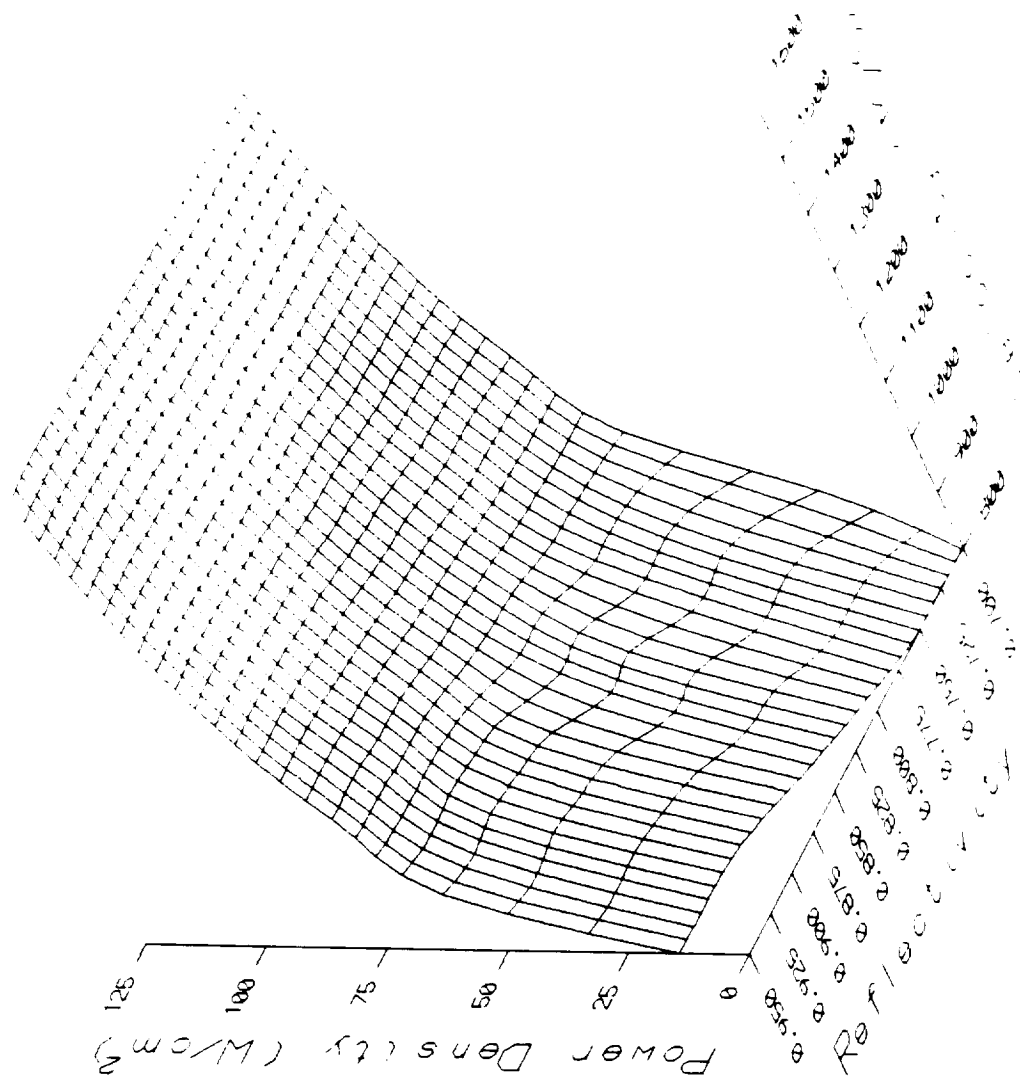


Figure C1 Power density vs velocity and reflectivity for t-C<sub>4</sub>F<sub>9</sub>I.



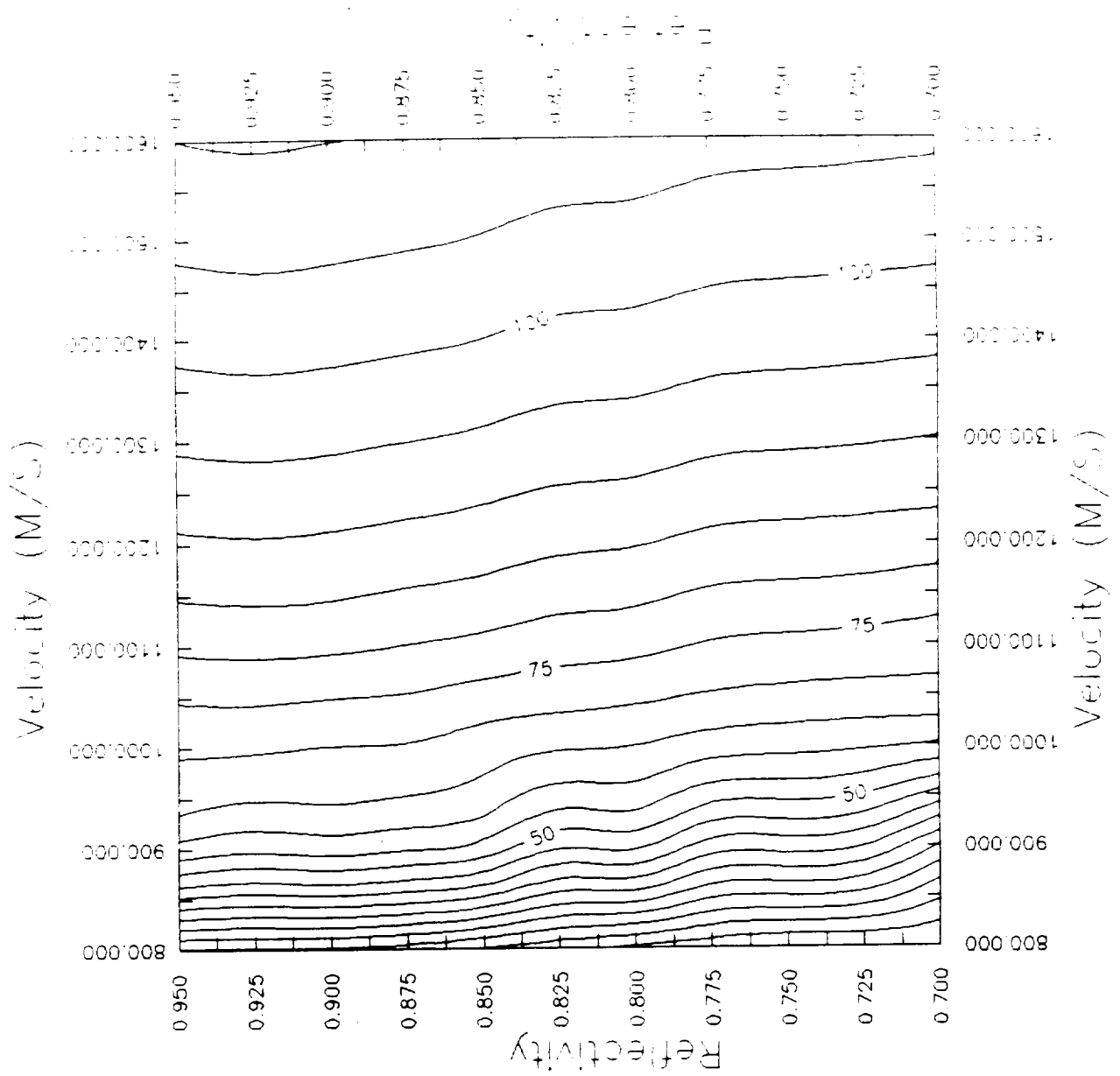


Figure C2 Level curves for power density in Figure C1.

FRAC = .0005

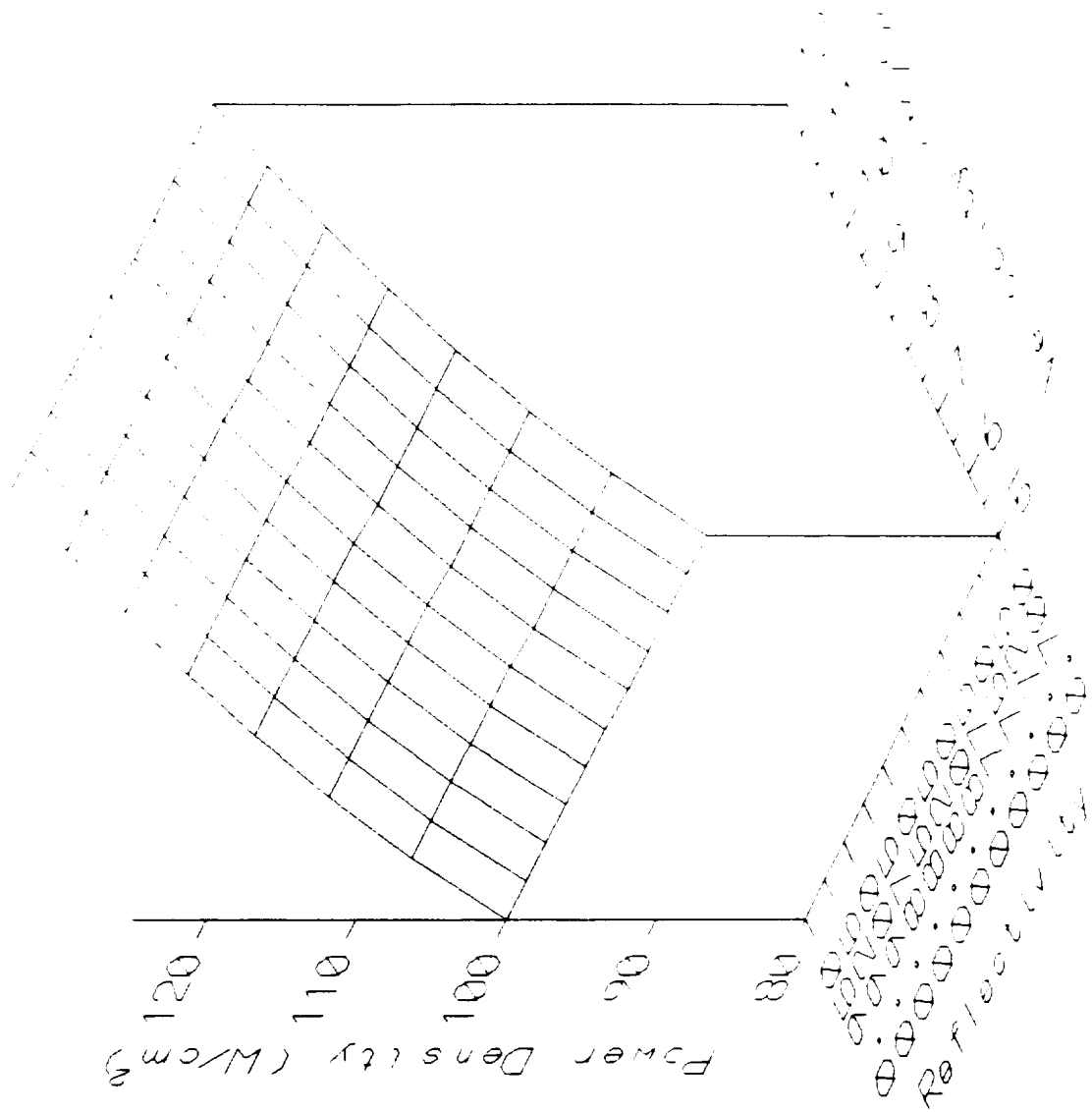


Figure C3 Power density vs velocity and reflectivity for t-C<sub>4</sub>F<sub>9</sub>I.

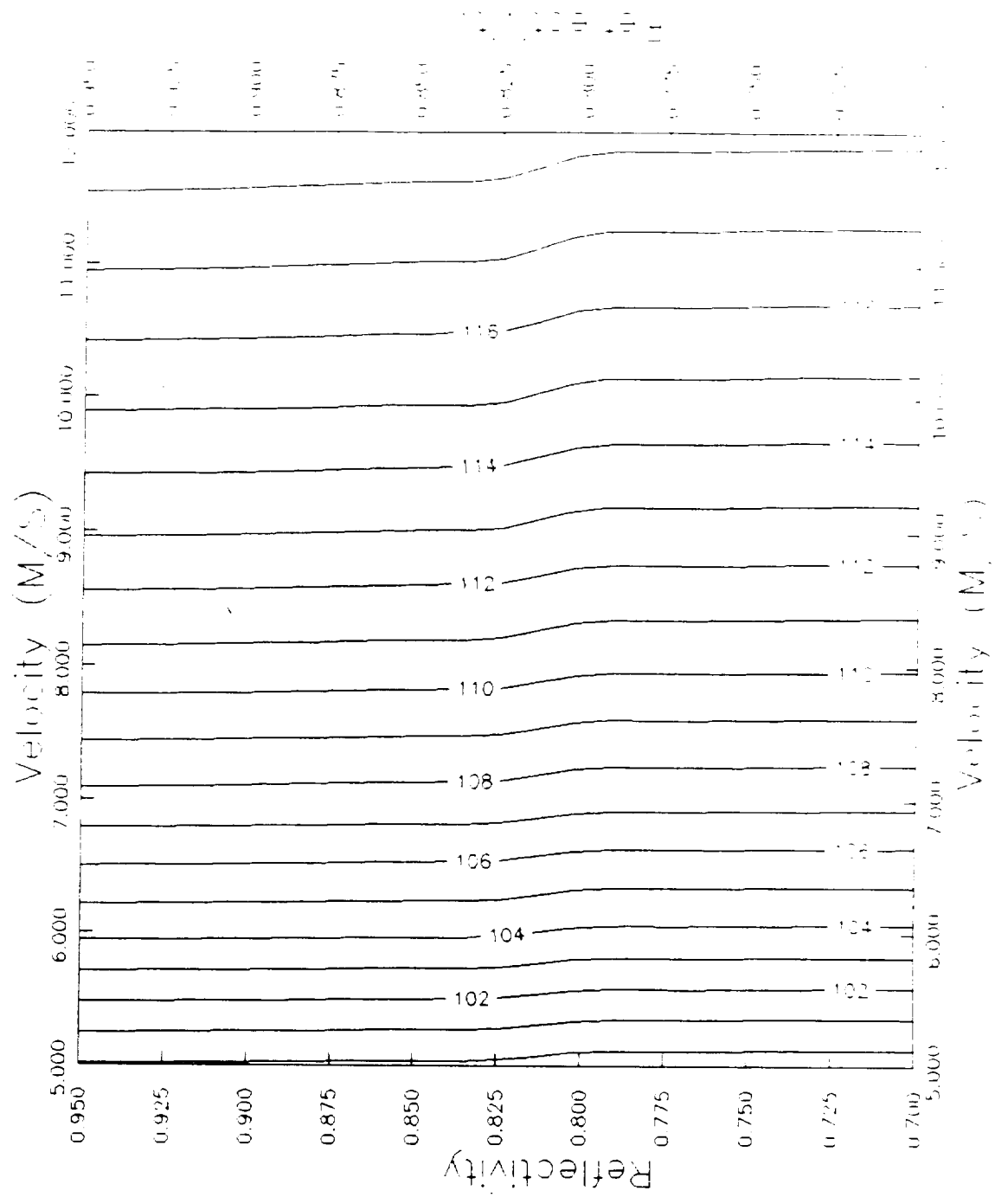


Figure C4 Level curves for power density in Figure C3.

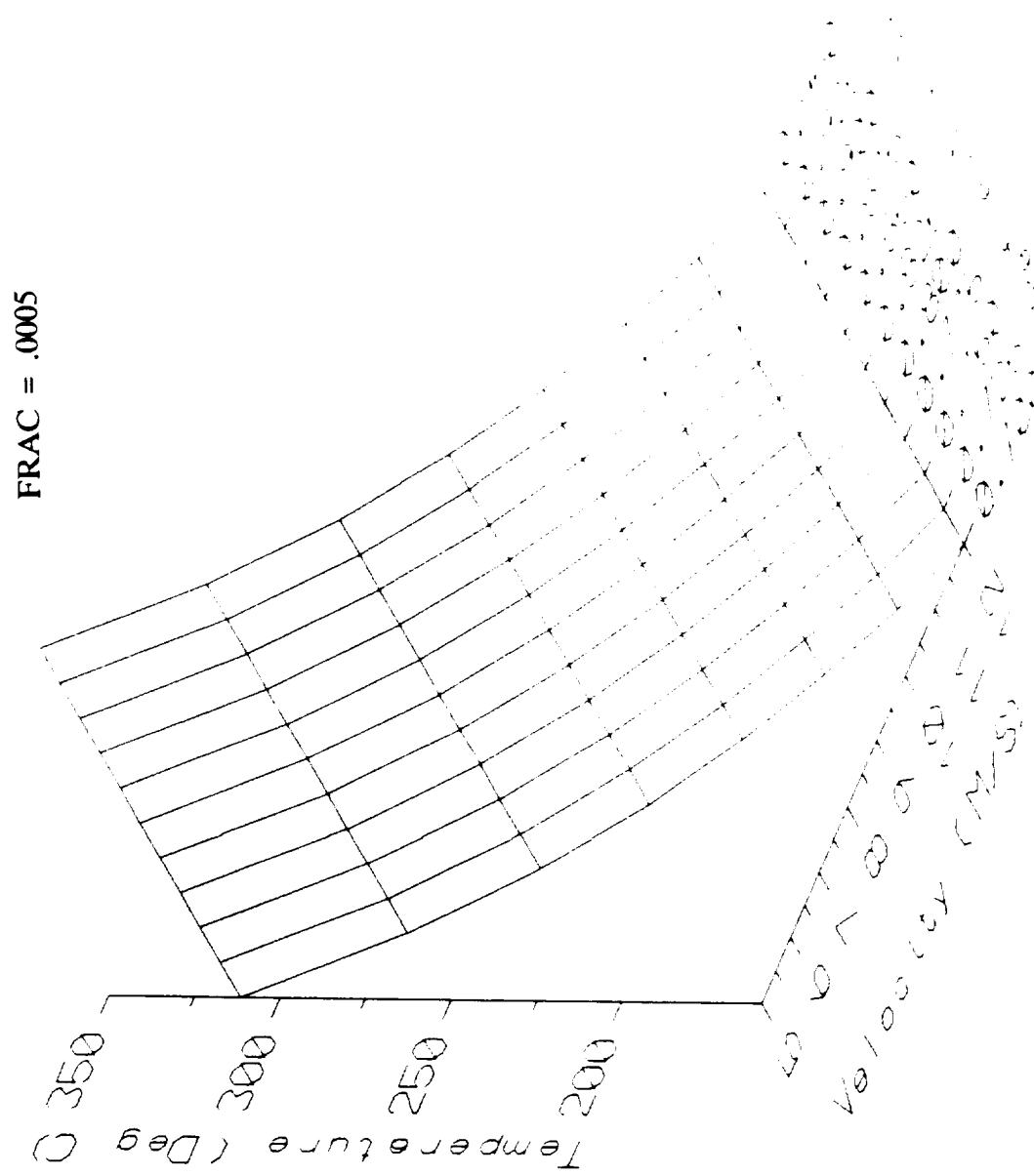


Figure C5 Temperature vs velocity and reflectivity for t-C<sub>4</sub>F<sub>9</sub>I.

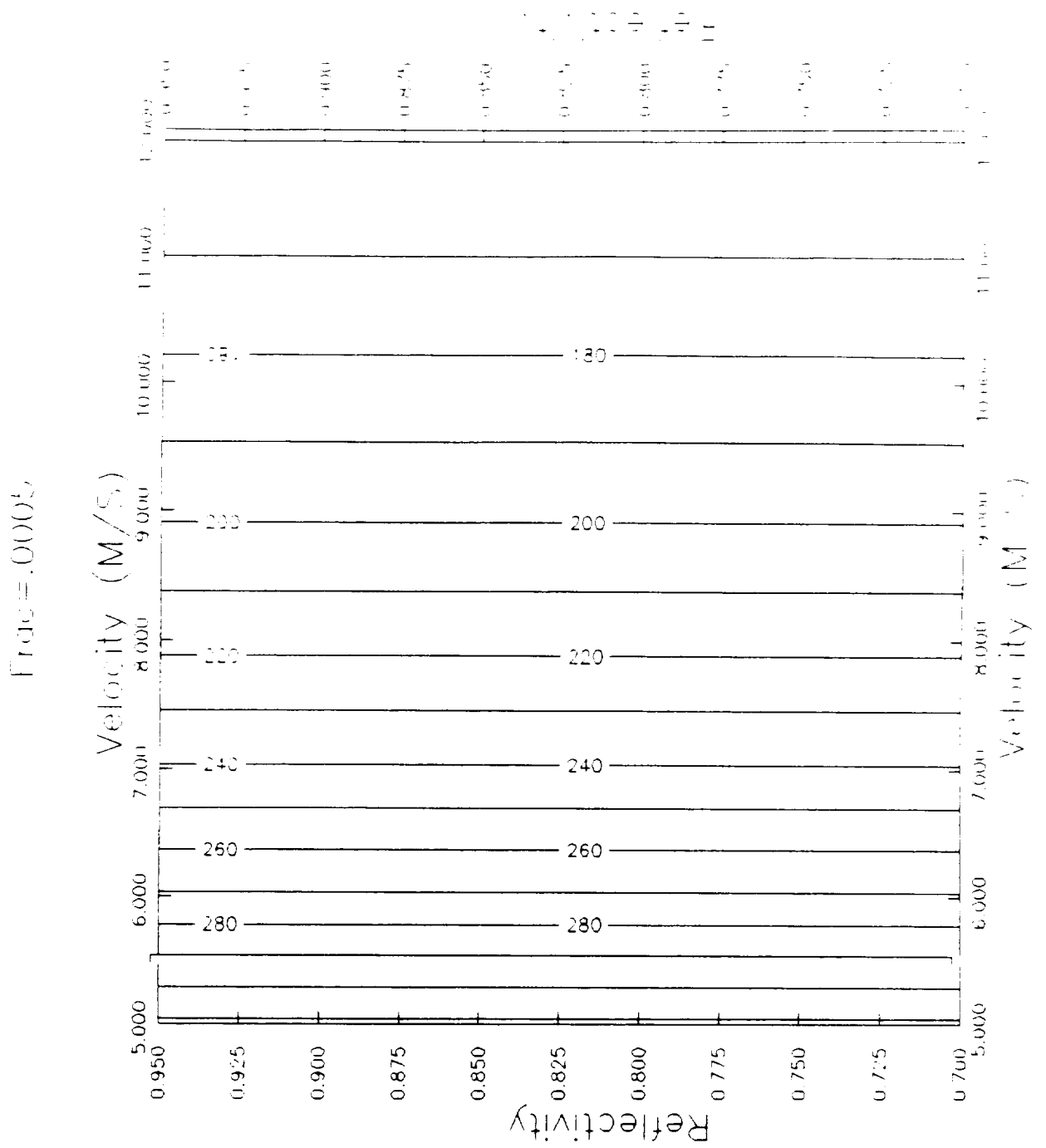


Figure C6 Level curves for temperature in Figure C5.

t-C<sub>4</sub>F<sub>9</sub>I with trace .001

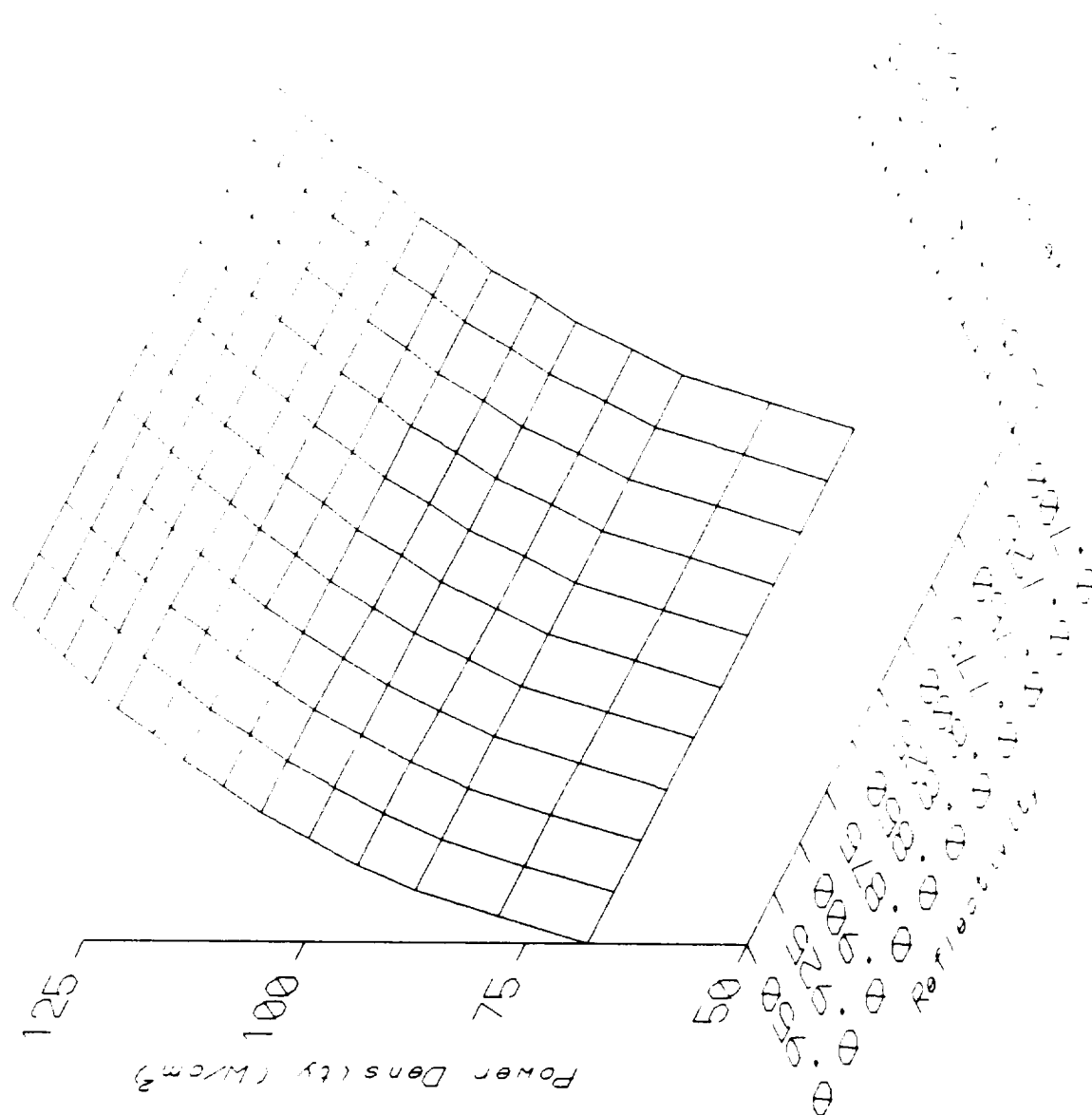


Figure C7 Power density vs velocity and reflectivity for t-C<sub>4</sub>F<sub>9</sub>I.

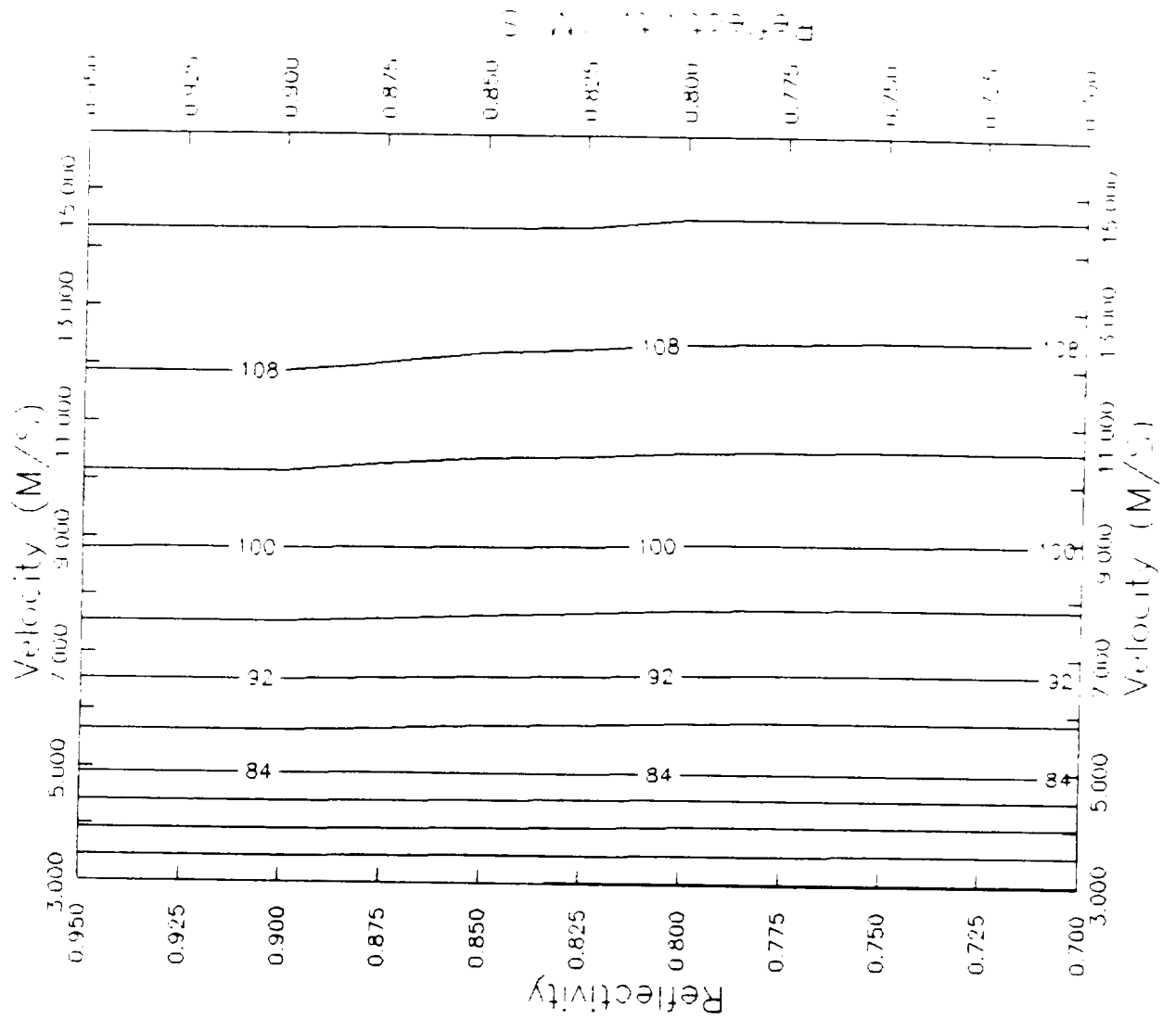


Figure C8 Level curves for power density in Figure C7.

t-C<sub>4</sub>F<sub>9</sub>I with trace O<sub>2</sub>

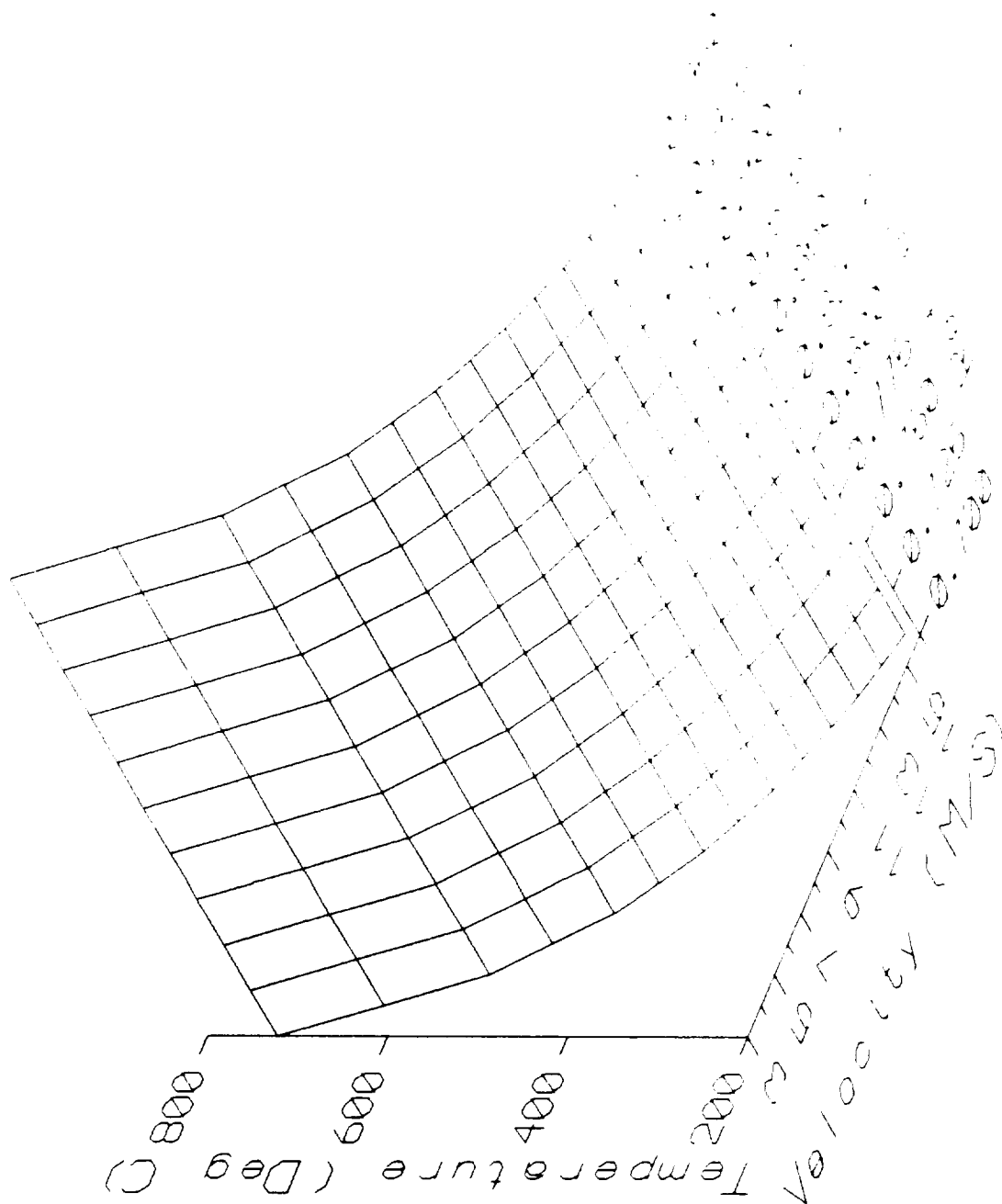


Figure C9 Temperature vs velocity and reflectivity for t-C<sub>4</sub>F<sub>9</sub>I.



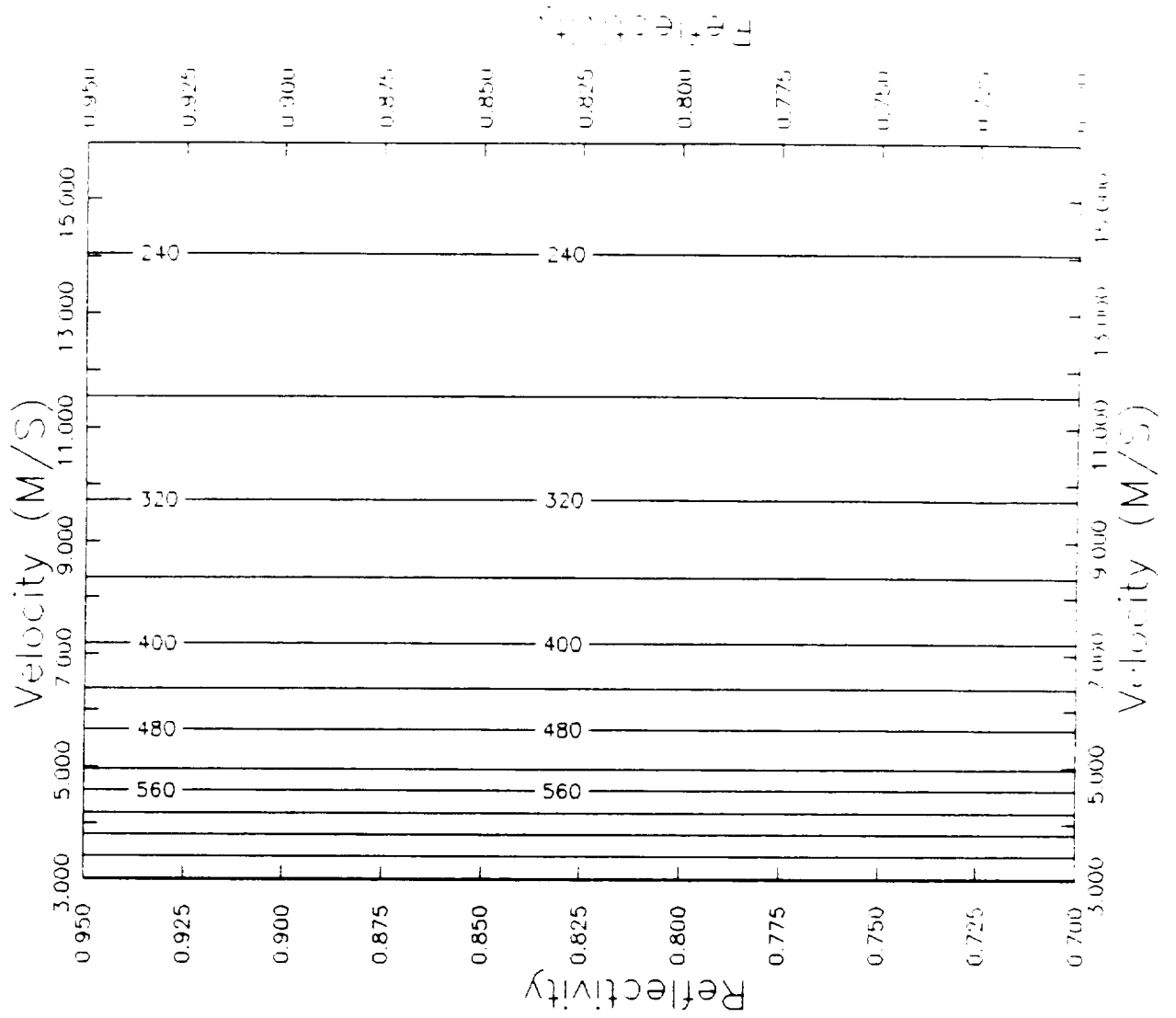


Figure C10 Level curves for temperature in Figure C9.